PHYSICAL REVIEW E **75**, 065302(R) (2007)

Experimental study of the bursting of inviscid bubbles

Frank Müller, Ulrike Kornek, and Ralf Stannarius
Institute of Experimental Physics, Otto-von-Guericke Universität Magdeburg, 39106 Magdeburg, Germany
(Received 28 February 2007; published 14 June 2007)

The rupture dynamics of smectic bubbles supported on a capillary is studied by means of microsecond photography, and properties of the retracting films are quantitatively analyzed. The film material collects in a moving rim that follows the sphere shape. A constant edge velocity is reached instantly; it is proportional to the inverse square root of the film thickness and in reasonable quantitative agreement with model predictions. The rim constitution for thin and thick films differs. In thin (submicrometer) films, the rim undulates and decomposes into single droplets, while for thick films, it remains compact and straight, and a brim is formed. During rupture, the initial film thickness increases globally, despite the smectic layer structure. Then, the recession of the film edge is accompanied by undulations of the bubble surface in the micrometer range.

DOI: 10.1103/PhysRevE.75.065302 PACS number(s): 47.20.Dr, 47.54.De, 47.55.dd

The rupture or collapse dynamics of thin liquid films has attracted the interest of scientists for more than a century, even long before such processes became accessible to direct experimental observation [1]. Rupture is driven by surface tension; the energy released by the surface reduction is converted into kinetic energy, and partly dissipated. Examples of such fast dynamical changes of topology are, e.g., the collapse of catenoid films [2,3] or the rupture of planar [4–6] or spherical [7,17] films.

When the reorganization of the initial film geometry is sufficiently slow, as in the collapse of bubbles or catenoids, the complete film material may be subject to flow. Caillier and Oswald [8] have studied the controlled deflation of half-spherical smectic bubbles. They found two competitive mechanisms: creation of islands of excess material, and continuous flow of film material into the meniscus. Dissipation connected with the latter process has been measured by Caillier and Oswald. Our experiments evidence that similar effects play a minor role in the much faster burst dynamics, and that the film far from the moving rim in first approximation can be considered at rest. During the rupture of plane films or bubbles, the forces driving the motion are assumed to act primarily on the rim surrounding a hole in the film. The dynamic processes are, at least in the commonly accepted models for inviscid films, essentially restricted to the rim. Even though global aspects of the rupture process are understood, most details of the properties of bursting films are unresolved so far.

Here, we consider the rupture dynamics of spherical free-standing films, initiated by the mechanical creation of a hole. When the hole starts to grow, the excess film material is collected in a quickly progressing rim. The rim velocity reaches a value where the energy gain from surface reduction is balanced by the increment of rim mass and dissipation in the rim. Rayleigh [1] calculated a limiting velocity of $v=\sqrt{4\sigma/\rho\delta}$ from the surface tension σ, the density ρ of the liquid, and the film thickness δ, under the assumption that all released surface energy is converted into kinetic energy. The first quantitative experiments seemed to confirm this relation [6], but later, Culick [9] and Taylor [10] independently retrieved a missing dissipation term in this model. From the more general momentum balance, they derived the rim velocity

$$v=\sqrt{2\sigma/\rho\delta}. \tag{1}$$

The kinetic energy reduces by a factor of 1/2, the rest of the released surface energy is dissipated. This holds irrespective of whether the rim is straight or circular in a flat film or whether it surrounds a hole in a spherical bubble. Pandit and Davidson reported experiments on the rupture of soap bubbles [7] and showed that the rim follows a spherical geometry with a time-independent velocity in quantitative agreement with Eq. (1). Their spherical films were spanned between two tubes; the average initial film thickness δ was estimated from previous resistance measurements. Effects in films of high viscosity have been considered experimentally and theoretically, e.g., in [11–13]. The viscosity effects reported in these papers can be excluded in the systems studied here.

We focus on smectic-*A* (Sm*A*) films, which have the advantage, compared to soap films, of an initially uniform thickness. The films are not subject to drainage. Film thicknesses can be varied in principle from two molecular layers (a few nanometers) to several micrometers. The bubbles studied here have radii of a few millimeters and thicknesses between ≈100 nm and ≈2 μm (several hundred layers). It is possible to determine the thickness optically before and during rupture [3]. Fast camera images were used to record the global rupture dynamics, and laser scattering experiments reveal transient structural changes of the membrane.

A sketch of the basic setup can be seen in Fig. 1(a). The bubble is illuminated with monochromatic light from a Schott light source collimated to a parallel beam. The rupture, lasting less than 10 ms, is recorded by means of an ultrafast camera (Photron Ultima APX), mounted on a long-range microscope (Infinity, K2). Our typical recording speed is 15.000 frames/s (fps), with shutter times of 1/120 ms to minimize haziness.

We use the standard liquid crystal (LC) 4′-octyl-biphenyl-4-carbonitrile (8CB), with the phase sequence $\mathrm{Cr} \overset{21.5\,^\circ\mathrm{C}}{\leftrightarrow} \mathrm{Sm}A \overset{33.5\,^\circ\mathrm{C}}{\leftrightarrow} N \overset{41.5\,^\circ\mathrm{C}}{\leftrightarrow} I$, where *N* indicates the nematic and *I* the isotropic phase. Experiments are performed at 26 °C, in the smectic *A* phase. The bubbles are prepared as follows: We draw a planar film on the end of a

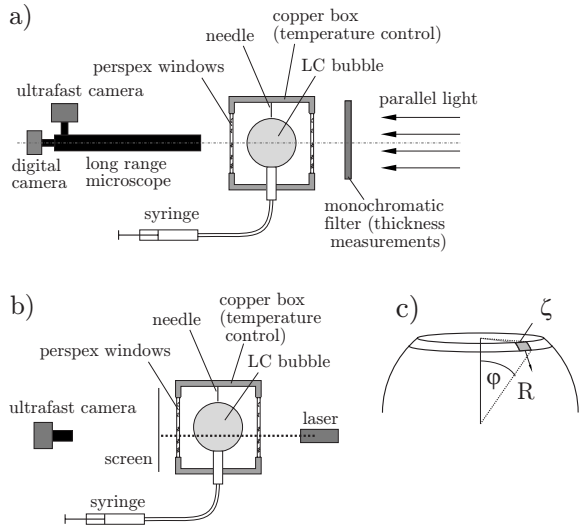

FIG. 1. Schematic drawing of (a) the basic experimental setup and (b) the laser scattering experiment; (c) sketch of the bursting geometry.

glass tube connected to a syringe. Air is pressed slowly into the bubble, which allows the film to grow at nearly uniform thickness; smectic material is constantly supplied from the meniscus. The film thickness can be influenced by the inflation speed. After inflation, the bubble is kept at rest until any possible thickness inhomogeneities have disappeared. In 8CB, the thinnest film region grows and finally covers the whole film; then the film thickness is uniform on a molecular scale. It is measured from the interference of monochromatic light ($\lambda \approx 535$ nm). The initial film is photographed with a Nikon digital camera. Comparison with calculated interference patterns [14] provides the initial thickness, for thick films ($\delta > 500$ nm) with an accuracy of ≈ 10 nm, for thinner films with an accuracy of ≈ 30 nm.

A modified setup is employed for the study of light scattering during the recession of the film. The bubble is probed by a laser beam pointing through the film [Fig. 1(b)] and the scattering profile is monitored on a screen at a defined distance from the bubble. The purpose of this experiment is to understand the dramatic optical changes observed in the transmission images during the burst (see below).

Rupture is initiated with a needle puncturing the bubble from the top. During the bursting we record either the transmission image or the laser reflex.

The expected rupture velocity follows from the momentum balance [9]. For a sphere of radius R, the tangential force on a rim segment ζ [Fig. 1(c)] is $F_t/\zeta = 2\sigma R \sin\varphi$, which changes the tangential momentum per segment, $\zeta^{-1} d(Mv)/dt$. The segment contains the film material of the corresponding hole sector, $M = \rho\delta R^2 \zeta(1-\cos\varphi)$. One arrives at the equation of motion $2\sigma R \sin\varphi = R^3 \rho\delta\, d^2/dt^2(\varphi - \sin\varphi)$, and the ansatz $\dot{\varphi} = \omega t$ yields a time-independent $\omega = \sqrt{2\sigma/(R^2\rho\delta)}$; see Eq. (1). Centripetal forces $R^3\zeta(1-\cos\varphi)2\sigma/\rho\delta$ necessary to keep the rim segment on a circular path are two orders of magnitude smaller than F_t. The dissipation is a consequence of the perpetual collision of the moving edge with film material at rest, which leads to nonspecific flow inside the rim.

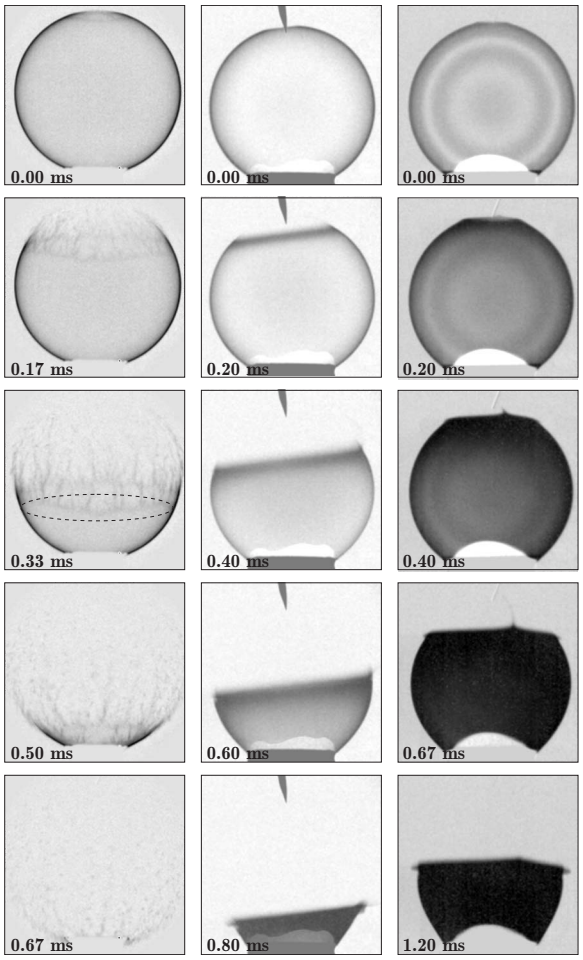

FIG. 2. Bubbles of different film thickness during rupture; film thicknesses are 100, 580, and 1460 nm, respectively (from left to right). The bubble radius is 4.5 mm in all cases. Note the obvious darkening of the transmission intensity during rupture in the thicker bubbles. All images have been background corrected and the contrast has been increased. The dashed curve indicates where the rim should be according to Eq. (1); see text.

Figure 2 shows image sequences of the rupture of bubbles with three different film thicknesses δ. Each column corresponds to a single experiment; time runs from top to bottom. The top images represent the first picture in the sequence after the rupture is initiated (<0.1 ms after puncture).

In accordance with the predicted δ dependence, the bubble in the left column ($\delta \approx 100$ nm) has disappeared completely after less than 1 ms, while the bubble with $\delta \approx 1460$ nm has only reached half-spherical shape after 1.2 ms. Before we treat the relation between rim velocity and film thickness in detail, the qualitative differences of the three experiments are discussed. Thin films (δ well below 500 nm) keep their transparent appearance during the complete rupture. The sensitivity of the high-speed transmission images is too low to detect film thickness changes of the order of a few layers, but if such phenomena occur, they are very small. The edge of the retracting film is unstable and shows a lateral modulation, with wavelengths in the submillimeter range. It rapidly decomposes into filaments and droplets.

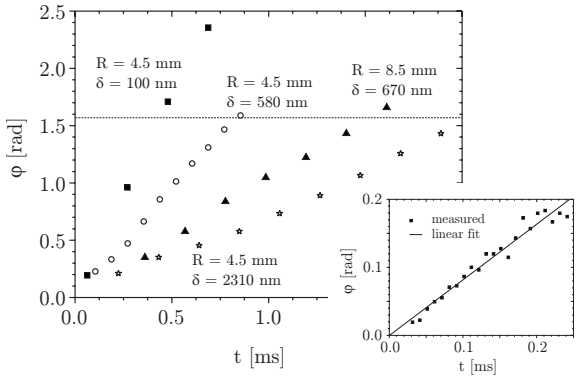

FIG. 3. Opening angle φ for selected bubbles as a function of time. Since we cannot determine the absolute start of rupture directly, $t=0$ is chosen from an extrapolation of the first images after puncture, under the assumption of a constant velocity, so that $\varphi(0)=0$. The horizontal line marks the hemisphere. Inset: $\varphi(t)$ obtained at a frame rate of 100 kfps ($R=4.6$ mm, $\delta\approx 1670$ nm).

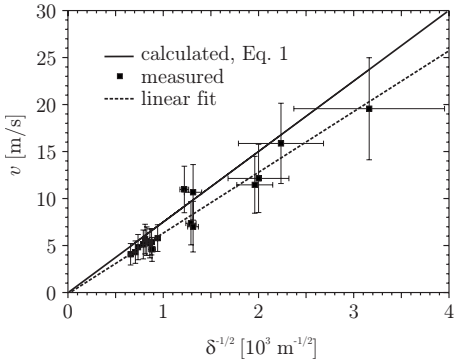

FIG. 4. Measured rim velocities. The solid line reflects Eq. (1) with literature data for ρ and σ. Experimental data are systematically lower by $\approx$20%; the dashed line is a linear fit.

Films of medium thickness (of the order of 0.5 μm) behave in principle similarly, but exhibit some new features. The rim moves more slowly and stays straight during recession. A darkening of the film in the vicinity of the moving rim is obvious. The front of the dark region moves faster than the rim. This optical change is even more pronounced in films of micrometer thickness and above (Fig. 2, right column).

In thick (micrometer) films, the bubble becomes completely opaque within the first millisecond after puncture. Before darkening sets in, one can still trace the interference fringes in the images and monitor film thickness changes. The fringes shift their positions outward, i.e., at least during the initial phase the bubbles increase their film thickness globally. The thickness increment is of the order of 10–30 nm. An exact quantitative determination of this change is affected by large uncertainties; in particular, there is no way to quantify film thickness changes after the film has become opaque. The darkening is a consequence of light scattering; it will be described below.

From the digital images, we obtain the angular velocity ω of the rim (Figs. 3 and 4). This velocity is constant within experimental accuracy for each bubble. An analysis of the initial rupture was performed at the highest available frame rate of 100 kfps, where we were able to monitor images of 128×32 pixels. The inset in Fig. 3 shows the initial 250 μs of the rupture process for a bubble of 4.6 mm radius and 1670 nm film thickness. The initial acceleration phase (if any) is beyond our experimental resolution, in the microsecond or sub-microsecond range.

The slopes of the graphs in Fig. 3 yield the (asymptotic) speed of the rim, $v=\omega R$. Figure 4 shows this velocity as a function of the inverse square root of the initial film thickness; data for different radii have been combined. The solid line reflects the dependence of Eq. (1) on the known material parameters of 8CB: $\rho=996$ kg/m^3 [15], and $\sigma=0.028$ N/m [16]. The measured velocities deviate from the model derived from momentum conservation by a factor of $\approx$0.8. Experimental values are systematically too low, particularly the more accurate data for thick bubbles. The dashed line in Fig. 2 gives an example of where the rim should be according to Eq. (1). The reasonable explanation is that part of the momentum is transferred to thin surrounding layers of air.

A further interesting aspect is the formation of a brim in thick bubbles, seen in Fig. 2 (bottom right pictures) and in detail in Fig. 5. Whereas in thin bubbles the rim consistently follows the spherical shape of the bubble remnant, the heavier rim in micrometer-thick bubbles folds outward. This instability needs further attention in the theoretical analysis of retracting edges of curved films; we expect that it is absent in planar films.

Finally, the origin of the darkening of transmission images (Fig. 2, right) is addressed. It depends remarkably on the initial film thickness. For films thinner than $\approx$300 nm, the effect is not measurable.

Since absorption can be excluded, we presume that structural changes, e.g., film undulations, lead to scattering of the transmitted light. In the transmission images, no undulations are resolved, thus one has to look for wavelengths in the micrometer and submicrometer range. We use the setup of Fig. 1(b) to record the scattering profile of a laser beam directed through the bubble. Initially, the laser covers a small circular spot on a screen at a distance of 57 mm from the bubble center [Fig. 6(a)]. After puncture, the scattering profile changes dramatically. A halo brightens up [Fig. 6(b)]. After that, when the rim passes the laser beam, the light intensity of the primary spot vanishes for a moment [Fig. 6(c)]. The final image is practically equal to the initial one. Thus, the interesting part is the intensity profile of the halo before the rim passes the laser beam. Scattering around the

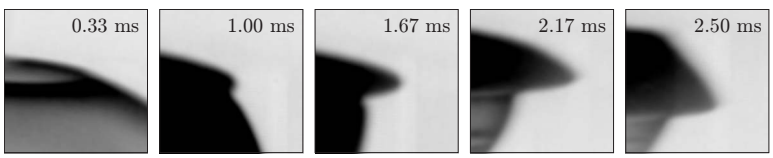

FIG. 5. Detail of the progressing edge in a bubble with $\delta\approx 1320$ nm during rupture. Such brims generally decorate films with $\delta>1$ μm, but even in films of 0.5–1 μm, a tendency to form small brims is observed.

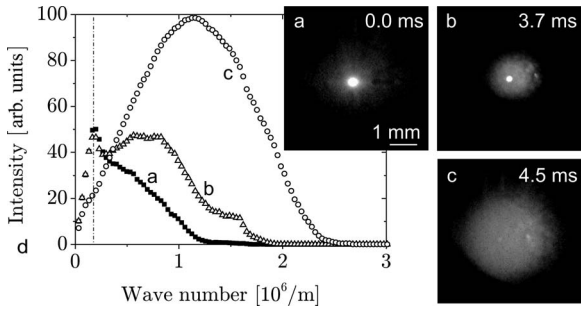

FIG. 6. Laser scattering profile (a) before and (b),(c) during rupture. The initial film thickness was $\delta = 1.4 \pm 0.1$ μm. (d) Radial scattering profiles before and during rupture. (c) corresponds to the instant when the rim reaches the beam. The primary beam intensity has been clipped in (d); the dashed line sketches the beam width.

primary beam is nearly isotropic; thus we sum up the intensities for equal wave numbers (on concentric circles around the primary beam). Figure 6(d) shows typical intensity profiles during rupture before the rim reaches the primary beam. The initial profile (solid symbols), representing the laser beam plus some static scattering in the setup, is shown for comparison. From the change of the profile we conclude that undulations of the film in the wave number range below 2 μm^{-1} dominate. The maximum is near $q \approx 1$ μm^{-1}, corresponding to $2\pi/q$ of the order of 5–10 μm. This maximum is relatively independent of the film thickness δ.

Summarizing, we have shown that the bursting of smectic-*A* bubbles can be described by Eq. (1), but experimental values are systematically 20% below the predictions. This is at the limit of experimental accuracy but seems to be significant. In thin (<0.5 μm) bubbles, the rim decomposes, whereas it remains straight and compact in thick bubbles. In thick films (>1 μm), a brim forms at the hole edge. During the initial phase of rupture, the global film thickness increases noticeably. The thickening is of the order of 10–30 nm; a clear dependence upon the initial film thickness could not be established. After that, the films scatter strongly, presumably by random film undulations. These fluctuations may be a consequence of the distortion of the smectic layer structure during the thickening of the films.

Support by DFG Grant No. STA 452/20 is gratefully acknowledged.

[1] J. W. Strutt, *Scientific Papers* (Cambridge University Press, Cambridge, 1899), Vol. 1, p. 474; (Cambridge University Press, Cambridge, 1902), Vol. 3, p. 441.
[2] S. A. Cryer and P. H. Steen, J. Colloid Interface Sci. **154**, 276 (1992); N. D. Robinson and P. H. Steen, *ibid.* **241**, 448 (2001); Y.-J. Chen and P. H. Steen, J. Fluid Mech. **341**, 245 (1997).
[3] F. Müller and R. Stannarius, Europhys. Lett. **76**, 1102 (2006).
[4] S. Frankel and K. J. Mysels, J. Phys. Chem. **73**, 3028 (1969).
[5] W. R. McEntee and K. J. Mysels, J. Phys. Chem. **73**, 3018 (1969).
[6] W. E. Ranz, J. Appl. Phys. **30**, 1950 (1959).
[7] A. B. Pandit and J. F. Davidson, J. Fluid Mech. **212**, 11 (1990).
[8] F. Caillier and P. Oswald, Eur. Phys. J. E **20**, 159 (2006). P. Oswald, P. Pierański, F. Picano, and R. Hołyst, Phys. Rev. Lett. **88** 015503 (2002).
[9] F. E. C. Culick, J. Appl. Phys. **31**, 1128 (1960).
[10] G. I. Taylor, Proc. R. Soc. London, Ser. A **253**, 313 (1959).
[11] M. Brenner and D. Gueyffier, Phys. Fluids **11**, 737 (1999).
[12] G. Debrégeas, P. Martin, and F. Brochard-Wyart, Phys. Rev. Lett. **75**, 3886 (1995).
[13] G. Sünderhauf, H. Raszillier, and F. Durst, Phys. Fluids **14**, 198 (2002).
[14] R. Stannarius, C. Cramer, and H. Schüring, Mol. Cryst. Liq. Cryst. Sci. Technol., Sect. A **350**, 297 (2000).
[15] D. Dunmur, M. Manterfield, W. Miller, and J. Dunleavy, Mol. Cryst. Liq. Cryst. **45**, 127 (1978).
[16] R. Stannarius and C. Cramer, Liq. Cryst. **23**, 371 (1997).
[17] G. Debrégeas, P. G. de Gennes, and F. Brochard-Wyart, Science **279**, 1704 (1998).